J Mater Sci: Mater Med (2016) 27:170
DOI 10.1007/s10856-016-5777-3

BIOMATERIALS SYNTHESIS AND CHARACTERIZATION

Original Research

Biocompatible nano-gallium/hydroxyapatite nanocomposite with antimicrobial activity

Mario Kurtjak[1,2] · Marija Vukomanović[1] · Lovro Kramer[2,3] · Danilo Suvorov[1]

Received: 29 May 2016 / Accepted: 2 September 2016 / Published online: 4 October 2016

Abstract Intensive research in the area of medical nanotechnology, especially to cope with the bacterial resistance against conventional antibiotics, has shown strong antimicrobial action of metallic and metal-oxide nanomaterials towards a wide variety of bacteria. However, the important remaining problem is that nanomaterials with highest antibacterial activity generally express also a high level of cytotoxicity for mammalian cells. Here we present gallium nanoparticles as a new solution to this problem. We developed a nanocomposite from bioactive hydroxyapatite nanorods (84 wt %) and antibacterial nanospheres of elemental gallium (16 wt %) with mode diameter of 22 ± 11 nm. In direct comparison, such nanocomposite with gallium nanoparticles exhibited better antibacterial properties against *Pseudomonas aeruginosa* and lower in-vitro cytotoxicity for human lung fibroblasts IMR-90 and mouse fibroblasts L929 (efficient antibacterial action and low toxicity from 0.1 to 1 g/L) than the nanocomposite of hydroxyapatite and silver nanoparticles (efficient antibacterial action and low toxicity from 0.2 to 0.25 g/L). This is the first report of a biomaterial composite with gallium nanoparticles. The observed strong antibacterial properties and low cytotoxicity make the investigated material promising for the prevention of implantation–induced infections that are frequently caused by *P. aeruginosa*.

1 Introduction

Gallium is a peculiar metal, with a low melting point (29.8 °C), a high boiling point (2200 °C), a very low vapour pressure, a descending solid–liquid isochore and a water-like freezing expansion [1, 2]. Its liquid droplets possess very high surface tension, but they wet many materials, like our skin or glass, due to the formation of an oxide layer on the surface [1–3]. Gallium nanoparticles (Ga NPs) possess many interesting properties, like optically induced phase transformation [4], extreme undercooling [5], or UV surface plasmon resonance [6]. In spite of all these intriguing properties, so far gallium has not been much used in practice, especially not in the nanometer-sized form. Gallium in the ionic (3+) state, on the other hand, has found many applications in medicine: for tumour imaging, hypercalcaemia treatment, bone-resorption inhibition, as an anticancer and an antimicrobial agent [7–9]. Among the other mechanisms, the antibacterial action of gallium ions is usually explained by the similarity between Ga(III) and Fe(III) ions. Ga^{3+} ions substitute Fe^{3+} ions, but cannot undergo one-electron reduction, so many important redox processes inside the bacteria are blocked [7, 9, 10]. Thus, the greatest effect was observed in strongly iron-dependent bacteria, like *Pseudomonas aeruginosa*, which can cause acute prosthetic joint infections and create biofilms on biomaterials [11].

Electronic supplementary material The online version of this article (doi:10.1007/s10856-016-5777-3) contains supplementary material, which is available to authorized users.

✉ Mario Kurtjak
mario.kurtjak@ijs.si

[1] Jožef Stefan Institute, Advanced Materials Department, Jamova cesta 39, Ljubljana 1000, Slovenia

[2] Jozef Stefan International Postgraduate School, Jamova cesta 39, Ljubljana 1000, Slovenia

[3] Jožef Stefan Institute, Department of Biochemistry and Molecular Biology, Jamova cesta 39, Ljubljana 1000, Slovenia

Antibacterial nanometals with antibacterial ions (such as Ag, Cu/CuO, ZnO) are known for a dual antimicrobial action of the nanoparticles and the released ions [12–15]. This dual action is expected from Ga NPs too as negative redox potential of gallium [2] should enable the release of the antibacterial Ga^{3+} ions. Following the idea of "nanobiotics" [16], the use of gallium nanoparticles instead of ions might lead to an enhanced, controlled, prolonged and local antibacterial action. However, their antibacterial properties have not been shown yet.

Based on the last claims, we were interested in the introduction of nano-gallium as a novel antibacterial component to a bioactive material, i.e., hydroxyapatite (HAp), which is widely used for bone/tooth implantation and tissue engineering [17–19]. This would result in a composite that could prevent infection and enable wound healing, tissue growth and repair around it. The Ag@HAp nanocomposite containing 10 wt % of Ag proved efficient against *E. coli* and *S. aureus* but toxic for IMR-90 human foetal lung fibroblast and U-2 osteosarcoma cells [20], while the specially designed Au/Arg@HAp nanocomposite was efficient and much less toxic [21]. Gallium has not yet been explored for such purpose. In contrast to silver or gold, gallium is effectively removed from the body through urine [22]. Metallic gallium is considered a safe chemical that is non-problematic for human health and environment [1, 23], but there are not many investigations on its cytotoxicity. One report warned about toxicity upon subcutaneous implantation [22] and there were several investigations on the gallium-based amalgams, where the cytotoxicity was connected with the corrosion and release of Ga^{3+} ions [24, 25]. Although the toxic values (for 50 % survival) of the released Ga^{3+} ions in these studies varied from 40 to 2000 µM depending on the cell line, cell number and the evaluation method, Ga was never among the most toxic released ions, always much less toxic than Ag^{+} and usually less toxic than Zn^{2+} [26–29]. One study also revealed that L-929 fibroblasts and MG63 osteosarcoma cells were able to proliferate and adhere on the Ti–Ga alloy containing 10 wt % of Ga [30]. Moreover, a recent study on eutectic GaIn alloy nanoparticles has shown their low in-vitro cytotoxicity against HeLa cells for at least 21 mg/L (0.2 mM Ga) concentration and their in-vivo injection into mice caused no tissue damage, no allergic reaction, exhibited very low acute toxicity (maximum tolerated dose of 700 mg/kg), while Ga and In were excreted with both faeces and urine [31].

The formation of Ga nanoparticles is a challenging task. Main currently existing methods require either reagents that are very sensitive to oxygen and water [32–34], or high temperature and ultrahigh vacuum [34–37]. On the other hand, a few recent articles describe an ultrasonic emulsification of liquid gallium into nanodroplets [38–41], which does not require such extreme conditions. All of the reported syntheses created gallium nanoparticles in colloidal suspensions or on a bulk substrate. So far, gallium was added to a bioactive material only in the ionic form, e.g., in bioactive glass [42–45] or in calcium phosphates [46, 47]. However, we found no literature on developing a composite of Ga NPs with a biomaterial.

In summary, the main hypothesis in this study is that gallium nanoparticles possess antibacterial properties, which are related to their dissolution and release of Ga^{3+} ions, so that by combining them with hydroxyapatite it is possible to create an applicable, biocompatible and effective antibacterial material. The aims of our work were to develop a new biomaterial, i.e., a nanocomposite made of gallium nanoparticles and hydroxyapatite (Ga@HAp), to characterize its physicochemical properties (structure, composition, morphology, release of Ga^{3+} ions) and to explore its antibacterial properties against *P. aeruginosa* and cytotoxicity for human lung fibroblast (IMR-90) and mouse fibroblast (L-929) cells.

2 Materials and methods

2.1 Synthesis methods

The Ga@HAp nanocomposite was created by a low-temperature ultrasonic emulsification in a Suslick flask. Gallium (99.99 % (trace metal basis), Acros Organics) was liquefied by heating above 30 °C and weighed in the liquid state (50 mg). The surface oxide layer on the Ga droplet was removed by a quick washing with 20 µL of 1M HCl [3]. 50 mL of ethylene glycol (spectrophotometric grade >99 %, Alfa Aesar), purged with N_2, were added and ultrasound pulses were provided with a length of 2 s, 80 % amplitude and breaks of 1 s for 3 h in a N_2 atmosphere and reflux. A 750-W sonochemical apparatus (Sonics & Materials) with a replaceable 13-mm tip was used as the ultrasound source. The ultrasonic horn was immersed 1.5 cm into the medium and the tip was 2.5 cm above the Ga droplet at the beginning. After 2 h of sonication, 10 mL of ethyleneglycolic suspension containing 70 mg of hydroxyapatite (prepared from $Ca(NO_3)_2$ $4H_2O$ (99.98 % (metals basis), Alfa Aesar) and $NH_4H_2PO_4$ (≥99.99 % (metals basis), Sigma-Aldrich) by the sonochemical homogeneous precipitation with thermal degradation of urea (99.3+%, Alfa Aesar) [48]) was added and the mixed suspension was further ultrasonicated with the same pulses. The resulting suspension consisted of Ga particles with wide size distribution from a few nm to 1 µm. However, the high viscosity of ethylene glycol (EG), stability of suspension of HAp nanorods in EG and absence of any interactions between large Ga particles and HAp nanorods enabled a separation of the Ga nanoparticles (diameter < 100 nm),

together with the HAp nanorods, from the larger Ga particles by centrifugation. After centrifugation at 5500 × g for 15 min, 80 % of HAp and the smallest Ga particles (20 % of the starting Ga amount) remained in the supernatant. This supernatant was mixed with three times larger volume of deionised water so that after centrifugation at 6300 × g for 15 min the Ga@HAp nanocomposite was sedimented. This sediment was re-suspended in acetone, centrifuged and dried. For the HAp sample the hydroxyapatite suspension in EG was mixed with water, centrifuged and dried in the same way as the Ga@HAp. Colloidal suspension of Ga NPs in EG was prepared by a 2-h ultrasonication of 50 mg of liquid Ga in 50 mL of EG under the same conditions as in the synthesis of the Ga@HAp, followed by a 15-min centrifugation at 5500 × g, after which the supernatant was retained and analysed.

The nanocomposite of silver nanoparticles and hydroxyapatite (Ag@HAp) was created by the reduction of $AgNO_3$ with $NaBH_4$ in the presence of hydroxyapatite [49]. 30 mg of $AgNO_3$ (99+ %, Alfa Aesar) were dissolved in 50 mL of water and mixed with 50 mL of an aqueous suspension of hydroxyapatite (70 mg). Then, 50 mL of an aqueous solution containing 80 mg of $NaBH_4$ (p. a. (≥99 %) $NaBH_4$, Fluka) were added and the mixing continued for 10 min. After this time, the suspension was centrifuged; the sediment was re-suspended in water, centrifuged again, re-suspended in ethanol and dried. The molar amount of $AgNO_3$ was the same as the molar amount of Ga in the Ga@HAp nanocomposite, so that 1 g of Ag@HAp nanocomposite contained roughly the same chemical amount of antibacterial component (2 mmol of nanoparticles per g of composite) as 1 gram of the Ga@HAp nanocomposite. The 2 mmol/g (24 wt %) content of Ag in the Ag@HAp was confirmed by the ICP-AES analysis.

2.2 Characterization methods

X-ray diffraction patterns were measured with an Empyrean X-ray diffractometer, from 4 to 70° with 100 s steps of 0.013° and Cu anode. FT IR analyses were made on a Perkin Elmer Spectrum 400 MIR spectrophotometer in the DRIFT technique for 2 mg of sample diluted with 70 mg of KBr. For the UV-VIS spectroscopy a UV-Vis-NIR Spectrophotometer Shimadzu UV-3600 was used. Transmission electron microscopy was done on a JEM2100 microscope with a LaB_6 electron source and Cu TEM grids with lacey carbon. The simulated electron diffraction pattern was calculated by the EMS software. Scanning electron microscopy was performed on a FEG SEM 7600F. The samples were dried on an Au-sputtered 100-nm filter membrane, stuck on the carbon tape and coated with 5 nm of carbon before the analysis. Bacteria were fixed onto such a membrane with glutaraldehyde, dehydrated and dried in critical point dryer (K850, Quorum Technologies) before sputtering with Pt/Pd. Phase-contrast and fluorescence images were recorded on a Nikon Eclipse Ti-U inverted microscope.

2.3 Ion-release study

A 0.2 g/L and a 0.5 g/L suspension of Ga@HAp in Mueller-Hinton (MH) broth (for microbiology, Sigma-Aldrich) and 0.5 g/L suspensions of the same material in 0.9 % NaCl and phosphate buffered saline (PBS, tablet, Sigma-Aldrich) were prepared. All suspensions were orbitally shaken for 24 h at 37 °C and 237 rpm. Then, the samples were centrifuged at 7000 × g for 15 min and the supernatants were further centrifuged at 15,350 × g for 15 minutes, after which the supernatants were filtered through a 0.1 µm filter. Concentration of Ga^{3+} in the filtered liquids was determined by the spectrophotometric method that is described in Section 2.5. The gallium content in the Ga@HAp before suspending in the media was also determined and the ratio of released/contained Ga was calculated as $\frac{m(Ga)released}{m(Ga)contained}[\%]=\frac{c(Ga)released}{w(Ga)\cdot c(Ga@HAp)}$ Thus, an average and standard deviation of this value was calculated from 3 parallel samples and 6 parallel samples in the case of the Mueller-Hinton medium (due to two different concentrations of Ga@HAp).

2.4 Quantitative determination of Ga

Six milligrams of the Ga@HAp nanocomposite were dissolved in 6 mL of 6 M HCl (prepared from 37 % HCl (for analysis, Carlo Erba reagents)) and diluted 100–200 times with 6 M HCl. The amount of Ga in the diluted sample was determined by a spectrophotometric method based on the absorbance of the $GaCl_4^-$–Rhodamine B complex [50]. The complex was formed in 4 mL of NaCl-saturated sample solution with 0.1 wt % of Rhodamine B and extracted to 4 mL of benzene (spectrophotometric grade (99.5+ %), Alfa Aesar). The standards for a calibration curve from 0.1 to 2 mg/L Ga concentrations were obtained by dissolving a measured mass of Ga in aqua regia, evaporating to dryness and dissolving the obtained white powder in 6 M HCl. The concentration of Ga^{3+} in the liquids of the ion-release study was determined by first mixing equal volumes (100–200 µL) of the liquid and concentrated (37 %) HCl, supersaturating with NaCl and then diluting with 6 M HCl and the Rhodamine B (Alfa Aesar) solution to a volume of 4 mL and extracting to 4 mL of benzene.

2.5 Microdilution antibiogram

Bacterial strains *P. aeruginosa* MW1 and PAO1 (wild type) were a gift from Dr. Matej Butala from the Biotechnical Faculty of the University of Ljubljana. For further details on

these two strains one may refer to [51]. An overnight culture of *P. aeruginosa* (MW1 or PAO1), prepared in microbiologically tested Miller Luria-Bertani broth (Sigma-Aldrich), was diluted 1000× with MH broth to obtain a concentration of 10^6 cfu/mL of bacterial culture. The dried material was suspended in MH broth and different dilutions were made in this medium from the stock suspension. Similarly, $Ga(NO_3)_3{\cdot}5.5\ H_2O$ (99.9 % $Ga(NO_3)_3{\cdot}xH_2O$, Sigma-Aldrich; the amount of water in the $Ga(NO_3)_3{\cdot}xH_2O$ was determined by the TGA analysis to be $x = 5.5$) was dissolved in the MH broth and filtered through a 0.1 µm filter, after which different dilutions were made with the sterile MH broth from the stock solution. Hundred microlitres of the suspension (or solution) were mixed with 100 µL of bacterial culture in a microtiter well and the flat-bottom Brand 96-well plate was incubated with 237 rpm orbital shaking for 24 h in a H1 Hybrid Multi-mode Microplate Reader (Synergy) while monitoring the absorbance (optical density) at 600 nm (OD600). Thus, the growth curves for all the samples were obtained and compared to determine the minimal inhibitory concentration (MIC). To eliminate the influence of the absorption by the materials, the absorbances of the corresponding sterile samples were subtracted from the signal of the samples with bacteria. To determine the bacterial concentration in the samples with $OD600 = 0$ after 24-h growth, the liquids above the materials were diluted 1000× and 50 µL of each liquid was spread onto a new MH agar plate (prepared from MH broth and agar for microbiology (Sigma-Aldrich)) and incubated for 24 h at 37 °C, after which the number of grown colonies was counted. For the antibacterial action assay of the released Ga^{3+} ions, the filter-sterilized liquids were mixed in different ratios with an overnight culture of *P. aeruginosa* MW1 and Mueller-Hinton broth, so that the bacterial concentration in the samples was $5{\cdot}10^5$ cfu/mL. Then, a microdilution antibiogram was performed in the same way as for the material suspensions and $Ga(NO_3)_3$. The average OD600 values and standard deviations were calculated from 4 parallel samples.

2.6 In-vitro cytocompatibility test

Cytotoxicity of the materials was tested on human foetal lung fibroblasts IMR-90 (ECCAC no. 85020204) and mouse fibroblasts L929 (ECCAC no. 85103115), which were grown in MEM (Gibco) supplemented with 10 % foetal bovine serum (Sigma), 2 mM L-glutamine (Invitrogen), 100 units of penicillin and 100 µg/mL streptomycin (Invitrogen) at 37 °C in a humidified 5 % CO_2 atmosphere. Ten thousand cells per well were seeded on a 96-well plate and grown overnight, then the growth medium was replaced with fresh medium containing dispersed particles and incubated for 24 h. To determine the remaining cell viability, growth medium was replaced with fresh medium containing 0.5 mg/mL 3-(4,5-dimethylthiazol-2-yl)-2,5-diphenyltetrazolium bromide (MTT) for two hours. The formed formazan crystals were solubilized in DMSO and transferred to a new transparent 96-well plate, where the absorbance at 570 nm was measured. Cell viability (%) was determined as the absorbance ratio between cells grown in presence and absence of the materials. The average values and standard deviations were calculated from 6 parallel samples.

3 Results

3.1 Characterization of the Ga@HAp nanocomposite

The synthesis of the Ga@HAp nanocomposite was repeated several times and five batches contained on average 16 ± 2 wt % of Ga, which indicates a good repeatability of the synthesis.

Ultrasonication of Ga in the absence of HAp leads to a colloidal solution of Ga nanoparticles in EG. These particles are spherical (Fig. 1a–c) and have a unimodal size distribution with a peak at 24 ± 2 nm and 50 % polydispersity (Fig. 1b). They exhibit a core-shell morphology, with a darker amorphous core and brighter amorphous shell (Fig. 1c). The EDS analysis on the Ga nanoparticles (Fig. 1b, c) confirmed the Ga phase. The ratio of intensities between Ga ($L\alpha_1$, $K\alpha_1$) and O ($K\alpha_1$) peaks was compared with such intensity ratio of these two elements measured in GaOOH and amorphous gallium hydroxide samples of very similar size and thickness and under the same EDXS measurement conditions. I_{Ga}/I_o ratio for Ga NPs was 7 times larger than for amorphous gallium hydroxide and 6 times larger than for GaOOH, which implies that the Ga NPs are not made of gallium oxide or hydroxide but rather of elemental Ga. The small oxygen signal might have come from a thin amorphous oxide/hydroxide shell on the surface of the Ga NPs. Ga has a strong tendency to passivate with a thin oxide film [3]. Previous investigations on Ga NPs have proven that the Ga core is covered with a thin oxide/hydroxide shell [6, 32, 33, 40, 52]. The electron diffraction (SAED) pattern on the Ga NPs consists of a ring, a diffuse halo and an almost invisible larger diffuse halo (Fig. 1b, d). These three rings match the three most intensive rings of the polycrystalline monoclinic β-Ga electron diffraction pattern. This indicates that the nanoparticles are made of a disordered β-Ga, which is actually liquid Ga [53]. The SAED pattern is almost identical to the previously reported elecron diffractions for liquid Ga nanoparticles [5, 33].

Morphologically, the Ga@HAp nanocomposite consists of HAp nanorods and spherical Ga nanoparticles attached to their surface (Fig. 1e–h). The Ga nanoparticles in the dried

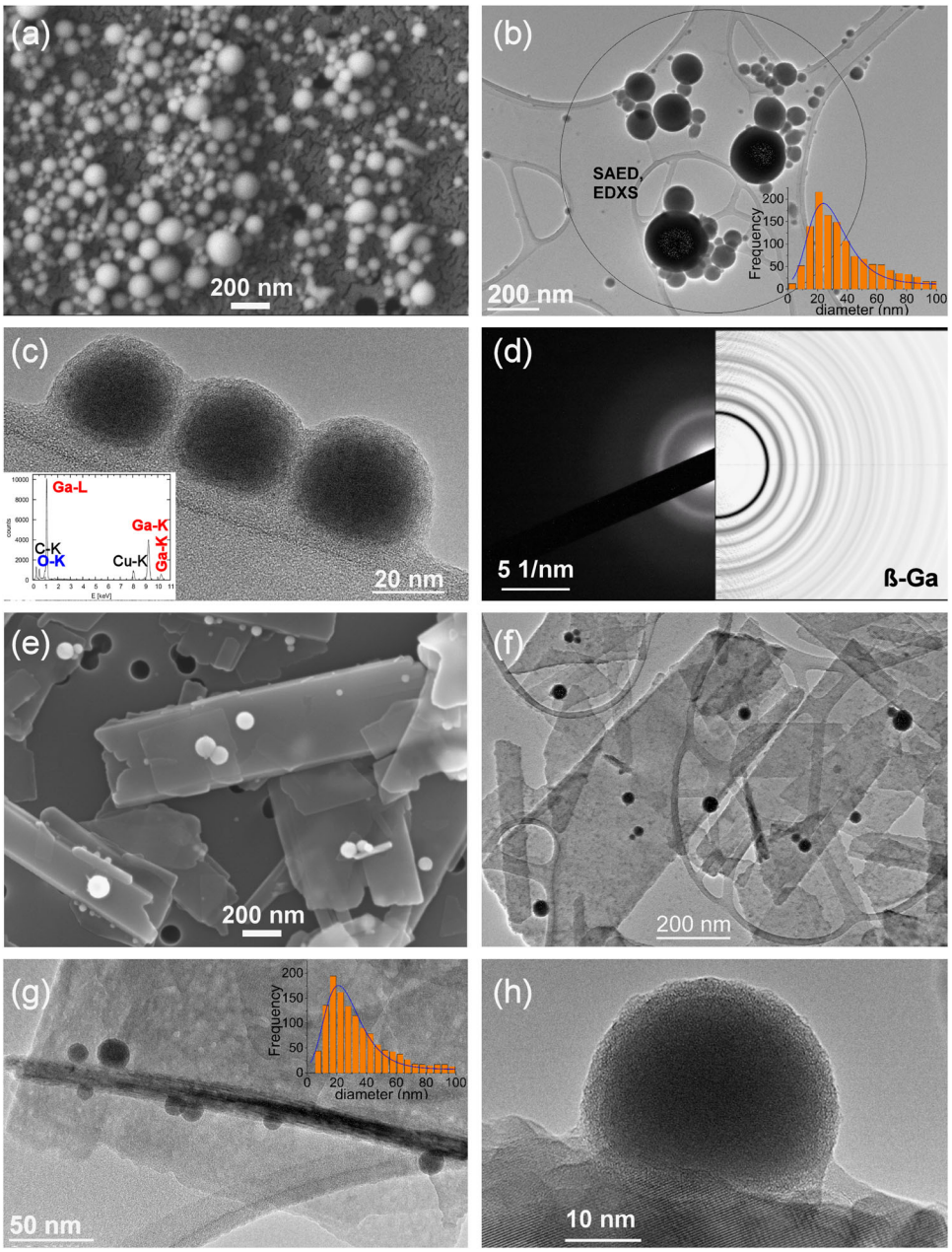

Fig. 1 Electron microscopy analysis. **a** SEM image of Ga nanoparticles (NPs) in ethylene glycol (EG); **b** TEM image of the Ga NPs, which were analysed by the EDXS and SAED, and the TEM size distribution of 1360 particles from the TEM images; **c** high magnification TEM of 3 Ga NPs in EG and EDXS analysis (*inset*); **d** SAED analysis of the Ga NPs with simulated electron-diffraction pattern for 24-nm β-Ga nanoparticles on the right-hand side (white background); **e** SEM image of the dried Ga@HAp nanocomposite; **f**, **g** TEM images of the Ga@HAp nanocomposite; the inset in **g** shows the size distribution of 1338 Ga nanoparticles on HAp based on the contrast in the TEM images; **h** high magnification TEM of a Ga nanoparticle on hydroxyapatite

nanocomposite are very similar to the colloidal Ga nanoparticles in EG. The size distribution of the Ga NPs in the Ga@HAp nanocomposite has a peak at 22 ± 2 nm and 50 % polydispersity (Fig. 1g). The HAp does not influence the ultrasonic dispersion of the liquid Ga and the size distribution of the so-formed Ga nanoparticles. However, there is an important difference between the colloidal Ga NPs and the Ga NPs in the Ga@HAp nanocomposite. While the colloidal Ga NPs are obviously agglomerated, the Ga NPs in the Ga@HAp nanocomposite are attached to the HAp nanorods and well separated. Hence, hydroxyapatite hinders their coalescence and agglomeration after the ultrasonication most likely by some electrostatic interactions that stabilize the Ga nanoparticles and compensate their surface charge. High-magnification TEM image (Fig. 1h) reveals the crystallinity of the HAp nanorod and no crystallinity for the Ga particles. In the Ga@HAp nanocomposite, part of the oxide/hydroxide layer on the Ga NPs might have come from the HAp, which can be concluded from the obvious wetting of the HAp surface by the Ga nanoparticle and the oxide layer deriving from the HAp.

The non-crystalline nature of Ga within the Ga@HAp nanocomposite was also confirmed by the XRD analysis. The diffractograms of both pure HAp and the Ga@HAp (Figs. 2a, b) show the diffraction maxima typical for the structure of the hexagonal apatite (PDF number of the

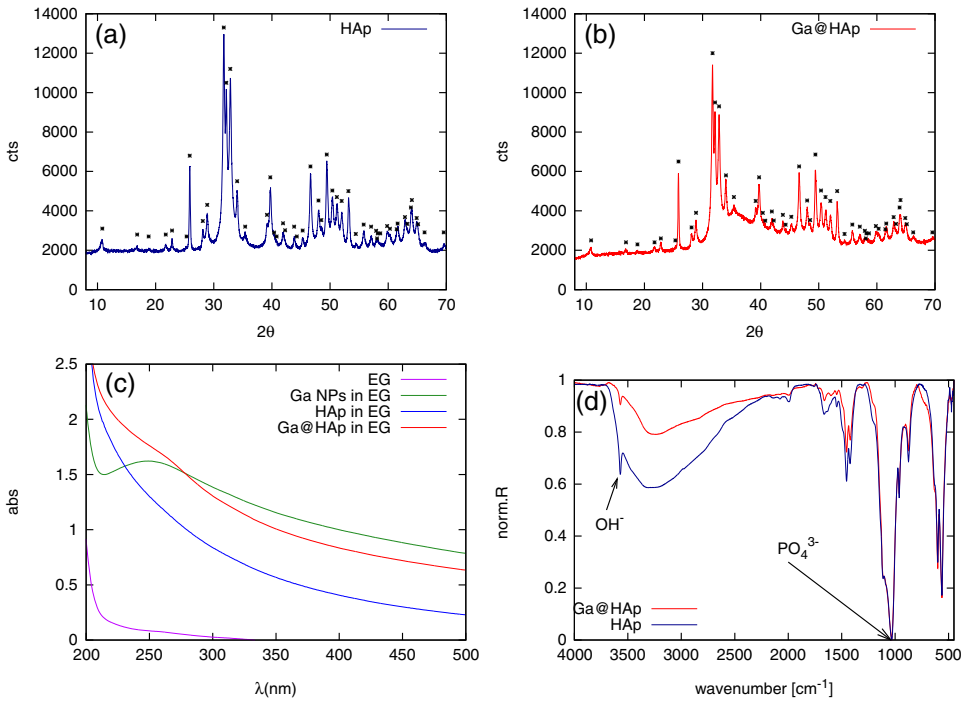

Fig. 2 Characterization of the Ga@HAp nanocomposite. **a**,**b** X-ray diffractograms of (**a**) HAp and (**b**) Ga@HAp. Asterisks (*) denote hydroxyapatite hexagonal (P63/m) reference pattern with PDF number 01-089-6438; **c** UV-VIS spectra of ethylene glycol (EG), Ga NPs in EG, hydroxyapatite (HAp) and Ga@HAp nanocomposite in EG; **d** IR spectrum of Ga@HAp in comparison with pure HAp nanorods. Both curves are normalized to [0,1]. The peaks due to OH^- and PO_4^{3-} vibrations in hydroxyapatite that were used for calculation of the OH/PO_4 ratio of heights are indicated with arrows

reference pattern 01-089-6438). There are no additional diffraction maxima that could be assigned to crystalline Ga, only an increased background between about 30 and 55° is observed for the Ga@HAp in comparison with the pure HAp. Based on our electron microscopy analysis and previous reports about the XRD of the Ga NPs [33, 40], it is reasonable to explain the raised background as a consequence of the presence of liquid (amorphous) Ga NPs in the Ga@HAp nanocomposite.

Another evidence that Ga nanoparticles are made of elemental Ga, is obtained from the optical properties. The UV-VIS spectrum of the colloidal solution of Ga NPs in EG contains a surface plasmon resonance (SPR) peak at about 250 nm (Fig. 2c). The SPR peak position agrees very well with a previous report [33] and with the calculated SPR peak by the Mie scattering theory [54] for 24-nm Ga NPs in a medium with a refractive index of 1.43 (ethylene glycol) and the optical constants for liquid gallium from the work of Knight et al. [6]. A similar peak can also be distinguished in the spectrum of the Ga@HAp nanocomposite as a shoulder superimposed on the absorbance curve of the HAp.

We investigated the type of interactions between the composite components by the FT-IR spectroscopy (Fig. 2d). The FT-IR spectrum of the pure HAp was compared to the spectrum of the Ga@HAp nanocomposite. Both spectra show all the bands due to the characteristic vibrations of the phosphate and OH groups for hydroxyapatite [48]. No chemical shifts or disappearance of the fine structure were noticed in the Ga@HAp sample, so we can exclude any chemical interaction between the Ga NPs and the HAp. There is a decrease in the intensity of the peak at 3600 cm^{-1} (the ratio of heights of the OH (3570 cm^{-1}) vs. the PO_4 (1032 cm^{-1}) peak was 4 times lower for the Ga@HAp in comparison with the HAp sample), which indicates existence of the interactions that block the stretching mode of OH-groups. Similar to previous investigations on interactions between HAp and Ag nanoparticles [55], blocking OH^- vibrations could be assigned to physical interactions between Ga nanoparticles and HAp. These interactions stabilize the formed Ga nanoparticles within the Ga@HAp nanocomposite and control their aggregation and further growth by their attachment onto the surface of apatite mediated by the surface OH-groups of HAp.

3.2 Antibacterial action against *P. aeruginosa* MW1 and PAO1

The antibacterial properties of Ga nanoparticles on HAp were examined with respect to the *P. aeruginosa* MW1 strain. Similar results were obtained for the PAO1 strain too. A qualitative disc diffusion test revealed that the Ga@HAp creates an inhibition zone, which is an indication of an antibacterial action. In the case of the HAp, tested as a negative control, no similar activity was detected (Supplementary Fig. S1). The survivability of the bacteria after incubation with the material was analysed using a fluorescent dye live/dead assay and revealed some bactericidal effect with clusters of dead bacteria observed for the Ga@HAp and not for the pure growth medium or HAp (Supplementary Fig. S2).

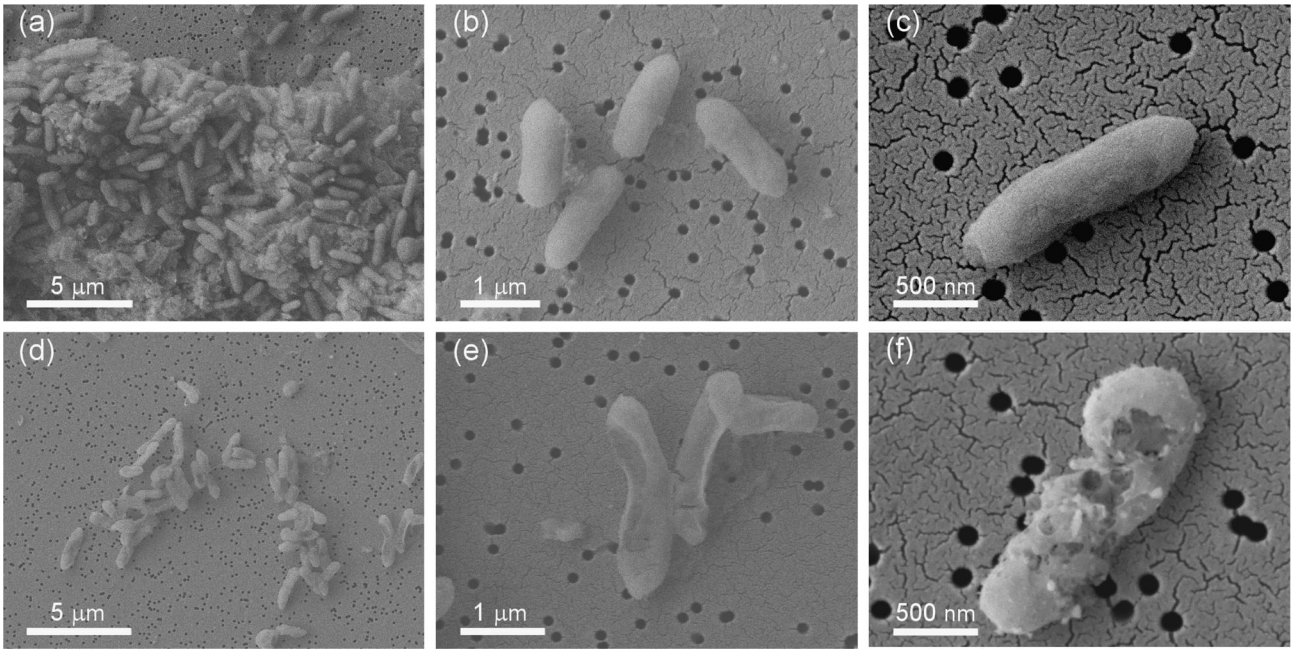

Fig. 3 Bacterial morphology. **a**, **b**, **c** SEM image of *P. aeruginosa* MW1 after 24-h incubation in growth medium with 0.5 mg/mL hydroxyapatite; **d**, **e**, **f** SEM image of *P. aeruginosa* MW1 after 24-h incubation in growth medium with 0.1 mg/mL of Ga@HAp

The morphological characteristics of the bacteria after a 24-h incubation with HAp and with Ga@HAp were observed under a scanning electron microscope (Fig. 3). The presence of the Ga@HAp during the bacterial growth led to a much lower number of bacterial cells and a decreased amount of well-preserved cells in comparison with the HAp (a negative control). In addition, a change in the structure of the dead bacteria was noticed. The dead bacteria that were exposed to the Ga@HAp exhibited holes in their cell wall and total rupture of the membrane, while the dead bacteria that were exposed to the HAp showed only a membrane/cell-wall integrity decrease.

The antibacterial action was quantified by a microdilution assay (Fig. 4). Normal 24-h planktonic growth results in an increase of the turbidity following a typical growth curve, which was monitored by measuring the absorbance at 600 nm (optical density or OD600). The Ga@HAp was tested in the concentration range from 0.01 mg/mL to 1.0 mg/mL with the pure MH growth medium and a 0.5 g/L HAp suspension as negative controls. The growth medium with no material, the HAp and Ga@HAp concentrations below 0.1 g/L show a distinct growth curve, while absence of such curve at higher concentrations represents a complete inhibition of growth (Fig. 4a). Hence, it is evident that the MIC for the Ga@HAp is at 0.1 g/L. For comparison, a nanocomposite of silver nanoparticles and hydroxyapatite (Ag@HAp; its morphology is presented in Supplementary Fig. S3) was also tested on the same bacteria and in the same conditions (Fig. 4b). The obtained MIC value for Ag@HAp (0.2 g/L or 0.4 mM Ag) was higher than the MIC value of Ga@HAp (0.1 g/L or 0.2 mM Ga). The 1000x diluted bacterial suspensions above the sedimented Ga@HAp samples after the microdilution test were spread onto a Mueller-Hinton agar plate and the grown colonies after a 24-h incubation at 37 °C were counted. A bactericidal effect was observed above the MIC value with a significant (1000×) reduction in the number of bacteria above 0.5 g/L (Fig. 5).

Ga^{3+} ions were released from the Ga@HAp nanocomposite in different physiological media during the 24-h shaking incubation at 37 °C and the ion release depended a lot on the medium (Fig. 6a). About 50 % of the contained Ga were released in the ionic form in the MH growth medium. By taking this fraction into account, about 0.1 mM concentration of Ga^{3+} ions emerged during the bacterial growth in the presence of 0.1 g/L of the Ga@HAp nanocomposite. Hence, the microdilution antibiogram of this sample was compared to the antibiograms of a similar concentration (137 μM) of Ga^{3+} ions only (released from the Ga@HAp in the MH medium) and a similar concentration of $Ga(NO_3)_3$ (141 μM, Fig. 6b). This concentration of Ga^{3+} ions alone, without the Ga@HAp sample, was not sufficient for the inhibition of growth. The MIC value that we obtained for $Ga(NO_3)_3$ against our *P. aeruginosa* MW1 strain, was 211 μM, while the MIC value for the released Ga^{3+} ions was 215 μM. Hence, the antibacterial

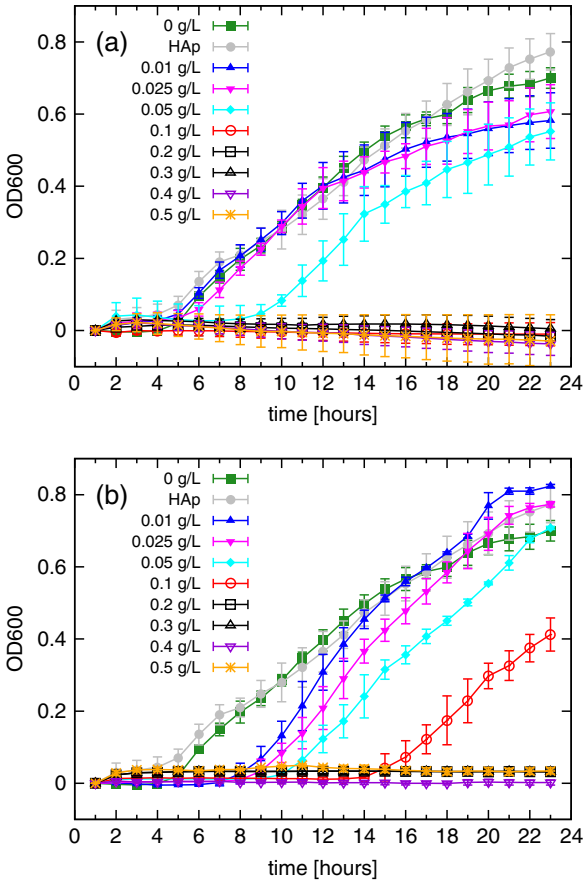

Fig. 4 Dilution antibiogram assay of **a** Ga@HAp and **b** Ag@HAp nanocomposite against *P. aeruginosa* MW1. Mueller-Hinton (MH) growth medium without any material (0 mg/mL) and 0.5 mg/mL HAp were taken as the controls

action of the Ga@HAp is not only a consequence of the released ions and nanoparticles are required to achieve the high efficiency of the Ga@HAp.

3.3 Cytotoxicity

After confirmation of the antimicrobial activity of the Ga@HAp biomaterial, the next task was the investigation of its interactions with mammalian cells. For that purpose in-vitro cell viability tests on IMR-90 human lung fibroblasts and L929 mouse fibroblasts (Fig. 7) were done. Different concentrations from 0.1 to 1 g/L were tested and the results for the Ga@HAp nanocomposite were compared with the HAp and the Ag@HAp and the minimal inhibitory concentrations of the Ga@HAp and the Ag@HAp. IMR-90 cell viability is high even for 0.5 g/L Ga@HAp, which is five times higher than MIC, and above 60 % at 0.75 g/L, while it drops to 50 % at 1 g/L (Fig. 7a). On the other hand, L929 survived very well also in the presence of the 1 g/L Ga@HAp (Fig. 7b). By contrast, the Ag@HAp nanocomposite (containing the same chemical amount of antibacterial substance) revealed toxic properties already very near its MIC value and decreased the survivability of L929 below 50 % at 0.25 g/L (Fig. 7b). Evidently higher toxicity of Ag@HAp in comparison with Ga@HAp was observed also for the IMR-90 cell line with around 60 % survivability at 0.25 g/L and below 50 % at 0.5 g/L (Fig. 7a). The observed cytotoxicity of the Ag@HAp is in agreement with the previously reported toxicity for Ag nanoparticles and Ag@HAp nanocomposite against L929 [56] and IMR-90 fibroblasts [20, 57]. All in all, Ga@HAp shows the desired

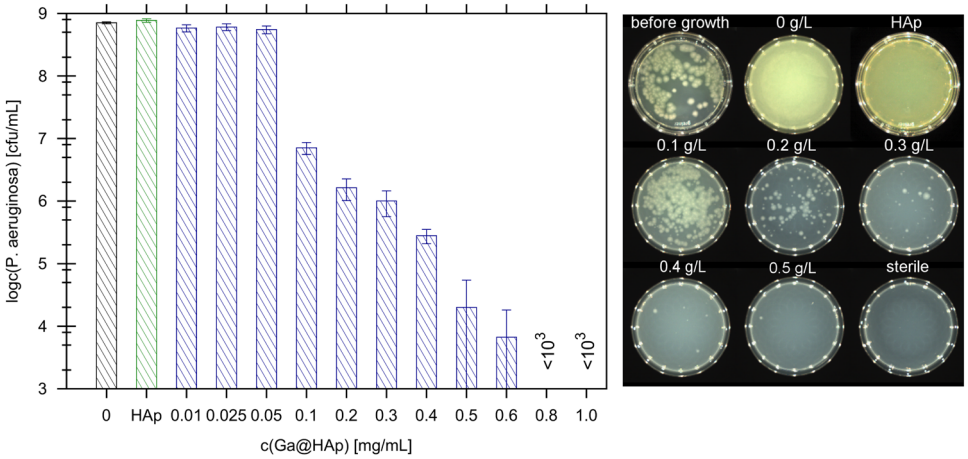

Fig. 5 Colony counting after dilution antibiograms. Bacterial concentrations on the left-hand image for the growth medium without any material (0), HAp and Ga@HAp concentrations below 0.1 mg/mL were calculated by multiplying the OD600 values with 1×10^9 cfu/mL. For higher Ga@HAp concentrations the bacterial concentration was obtained by diluting the liquids above these samples after the 24-h microdilution assay (Fig. 4) 10^3 times, smearing 50 µL onto the Mueller-Hinton (MH) agar plates and colony counting after incubation for 24 h. The representative agar plates with colonies are shown in the right-hand image. Sterile MH growth medium (sterile), growth medium with *P. aeruginosa* and without material (0 g/L) before (5×10^5 cfu/mL) and after the microdilution antibiogram, and 0.5 g/L HAp are put for comparison

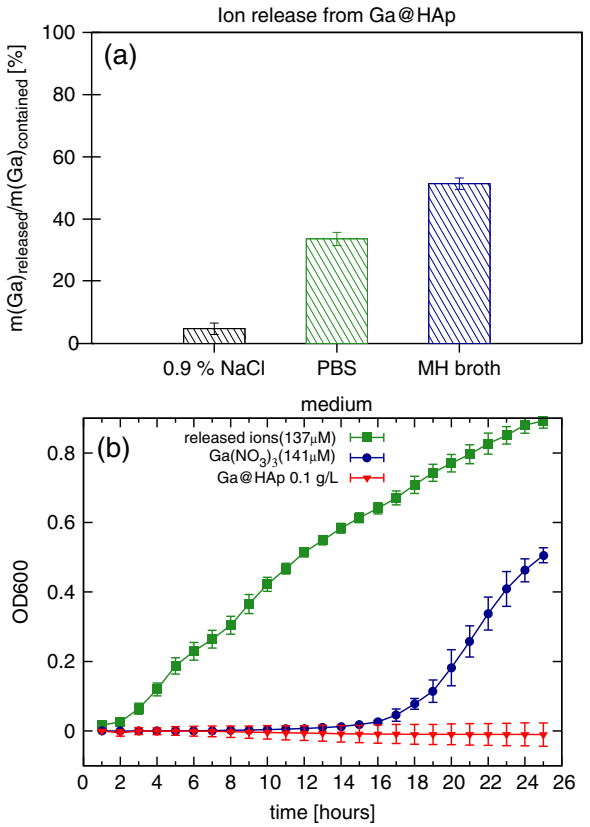

Fig. 6 Ion release assay. **a** Fraction of the contained Ga in the Ga@HAp that was released after 24-h shaking at 37 °C in three different media: 0.9 % NaCl, PBS and Mueller-Hinton (MH) broth; **b** a comparison of the antibacterial action of the released ions in (MH broth) from the Ga@HAp nanocomposite, $Ga(NO_3)_3$ and the according Ga@HAp that releases a similar amount of Ga^{3+} ions. Similar molar concentrations of Ga^{3+} were chosen for all three samples and a 50 % release of Ga^{3+} was assumed for the Ga@HAp sample

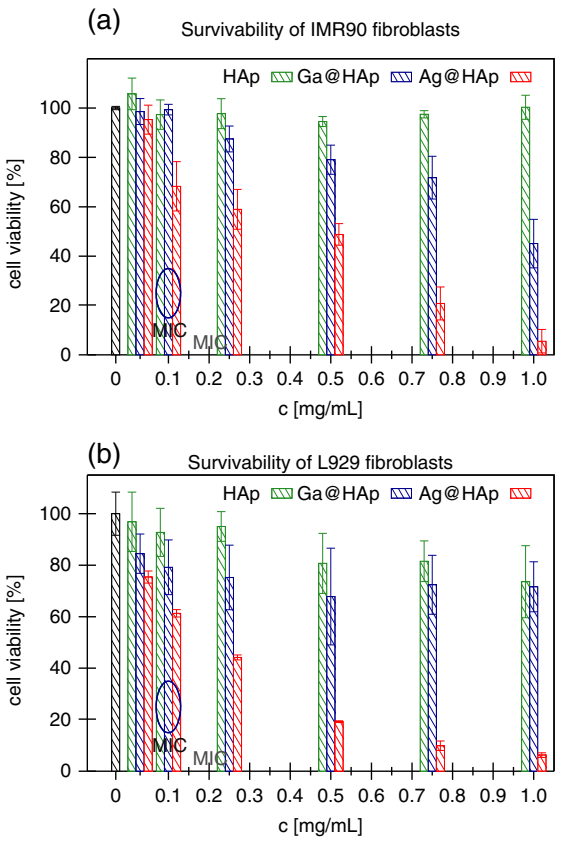

Fig. 7 Cytotoxicity assays. **a** Survivability of IMR-90 human lung fibroblasts after 24-h growth in the presence of the HAp (green or first columns from the left), Ga@HAp (blue or the middle columns) and Ag@HAp (red or third columns from the left) materials; **b** Survivability of L929 mouse fibroblasts after 24-h growth in the presence of the HAp (green or first columns from the left), Ga@HAp (blue or the middle columns) and Ag@HAp (red or third columns from the left) materials. Minimal inhibitory concentration (MIC) at 0.1 g/L for *P. aeruginosa* MW1 of the Ga@HAp nanocomposite is circled and indicated in blue while the MIC of the Ag@HAp at 0.2 g/L is indicated in red

properties of antibacterial action and low cytotoxicity in the concentration range from 0.1 to 1 mg/mL and it proved a better option than the Ag@HAp nanocomposite with antibacterial action and low cytotoxicity in the concentration range from 0.2 to 0.25 mg/mL.

4 Discussion

Since we wanted to keep the desired properties of the hydroxyapatite, such as its nanocrystallinity, bioactivity, and the active surface for the attachment of nanoparticles, the high temperature, high vacuum and water-sensitive reducents were avoided. Therefore, we found the ultrasonic emulsification method the most suitable for developing the Ga@HAp nanocomposite. To isolate the antibacterial activity of the Ga NPs from any possible antibacterial activity of a surfactant and to avoid any toxicity induced by such surface modification, the use of any surface-active agent was deliberately avoided. This resulted in a relatively wide size distribution, yet the antibacterial action and biocompatibility was confirmed. The characterization revealed that the Ga particles were generally smaller than 100 nm (with a unimodal size distribution and the majority of particles in the range of 22 ± 11 nm), liquid/amorphous, coated by a thin amorphous oxide/hydroxide shell and well separated due to weak attachment to the surface of the hydroxyapatite.

Our hypothesis for the antibacterial properties of Ga nanoparticles was based on the known antibacterial action of gallium ions, the connection between antibacterial nanometals and their antibacterial ions, and the thermodynamically favorable oxidation of Ga to Ga^{3+}. However, since the oxidation of Ga ends within a thin oxide layer, it was questionable as to whether the observed antibacterial

action is really connected to the release of gallium ions, or whether the gallium nanoparticles have a different mechanism for the prevention of bacterial growth. Our ion-release study has shown that 1/3 of Ga in the nanocomposite is dissolved during 24-h shaking incubation at 37 °C in PBS, while 1/2 of the contained Ga is released as Ga^{3+} ions during a similar incubation in the MH growth medium. This proves the expected release of ions. The next question that arises is whether Ga nanoparticles or only the released ions are antimicrobial. Since there are many different MIC values against *P. aeruginosa* reported for ionic gallium [58, 59], depending on the strain, the growth medium and the gallium species, we rather compared the MIC for Ga@HAp with the MIC value of the released ions and the MIC value of $Ga(NO_3)_3$ that were obtained in our study. The MIC for the Ga@HAp nanocomposite is at 0.1 mg/mL, which corresponds to about 0.2 mM Ga. This agrees well with the MIC of $Ga(NO_3)_3$ at 211 µM. However, our ion-release study revealed that only 50 % of the contained Ga in the Ga@HAp is released as ions after 24 h of incubation, which yields 0.1 mM concentration of Ga^{3+} that alone is not sufficient for the complete inhibition of growth. Therefore, the antibacterial action of the Ga@HAp nanocomposite cannot be explained only by the antibacterial action of the released ions. There are three possible antibacterial sources: the Ga nanoparticles, the oxide shell or the Ga ions formed by the dissolution of the Ga nanoparticles (Fig. 8).

If the antibacterial properties come only from the release of ions, then the mechanism of antibacterial action is known and the Ga nanoparticles serve as reservoirs and deliverers of Ga ions, while their dissolution would also be a way for their elimination from the body. The observed large extent of dissolution of Ga NPs in the absence of any cells and the fact that the antibacterial and cytotoxicity properties were well repeatable despite the wide Ga size distribution go in favour of this mechanism.

However, although the contribution of the nanoparticle to the antibacterial action apart from the ion release is still debatable in metallic nanoparticles, such as Ag nanoparticles [60], this possibility should not be excluded. Especially, because it obviously contributes at least to improved transport of Ga^{3+} ions into bacteria. The destruction of bacteria (the holes in cell membranes of the dead bacteria), observed under SEM, is an indication of the effect of nanoparticles, which is often (but not always) connected with the generation of reactive oxygen species (ROS) [61]. However, non-selective extracellular release of ROS is not expected for Ga nanoparticles under the studied conditions and the observed low cytotoxicity is also an indication against such mechanism. A recent investigation has proven that Ga_2O_3 nanoparticles do not produce any ROS in water without direct ultraviolet or visual light illumination [62]. Moreover, unlike Ag or Cu [63–65], Ga

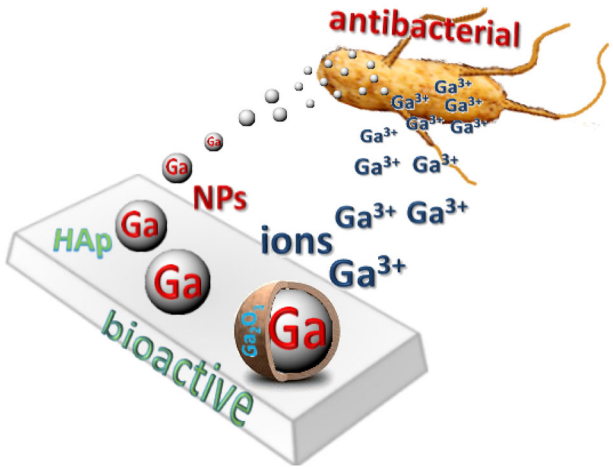

Fig. 8 A graphical summary of the diverse properties of the Ga@HAp biomaterial and the proposed sources of its antibacterial action

cannot undergo Fenton-like reactions that lead to ROS. Instead, the endocytosis, fusion and dissolution of Ga nanoparticles without causing cytotoxicity could occur in a similar way as was observed for the GaIn eutectic nanoparticles in HeLa cells [31]. On the other hand, intracellular ROS could be caused indirectly by the released Ga^{3+} ions as a consequence of the Ga^{3+}-Fe^{3+} substitution inside the cells, as was shown for gallium nitrate and citrate, the FDA approved drugs, in *Pseudomonas* bacteria as well as human lymphoma cells [66, 67]. Since avoiding non-selective extracellular toxic ROS might be the greatest advantage of Ga nanoparticles over the existing antimicrobial nanomaterials in search of an efficient antibacterial protection that would not be harmful to mammalian cells, a more detailed insight into the mechanism of antibacterial action of Ga nanoparticles and generation of ROS seems a reasonable task in further investigation.

Finally, if the gallium oxide layer is responsible for bacterial inhibition, the main question is whether the Ga_2O_3-coated Ga NPs have any advantages over Ga_2O_3 NPs, which have not yet been shown to prevent the planktonic growth of *P. aeruginosa*.

All three suggested mechanisms are probably connected in the Ga@HAp: the Ga NPs, the gallium oxide/hydroxide shell and the release of ions, with the major part coming from the ion release. Sahoo et al. explored the antibacterial properties of GaN nanoparticles on *Pseudomonas* strains and explained their mechanism by local damage of the cell wall, caused by nanoparticles, which led to leakage of intracellular components, and a possible release of Ga^{3+} ions inside the bacterial cells [68]. On the other hand, Lu et al. have shown endocytosis, fusion and degradation of the eutectic GaIn nanoparticles with release of Ga^{3+} ions inside HeLa cells [31]. In this view, the high efficiency and the low cytotoxicity of the Ga@HAp nanocomposite can also

be explained only by the local release of Ga^{3+} ions from the Ga nanoparticles in the vicinity of the nanocomposite and bacteria or even inside the bacteria. Further investigation will be needed to confirm or reject these hypotheses. The investigation of the mechanism will require a narrow size distribution of the Ga NPs, since the suggested mechanisms are most likely size-related. It is known that solubility increases with decreasing size of the particles [69, 70]. However, Ga nanoparticles, coated with amorphous oxide/hydroxide offer another parameter that affects their dissolution, i.e., the thickness of the oxide/hydroxide shell. Hence, the release of ions might be controlled by the size of the Ga nanoparticles and the thickness of the oxide/hydroxide layer. Based on the ion-release mechanism, the antibacterial action would also be controlled by these two parameters. We have done some preliminary tests (data not shown) that revealed higher MIC values for the Ga@HAp materials with wider size distributions (obtained by shorter ultrasonication and without separation of particles by centrifugation) at the same Ga content. Thus, we believe that the narrower size distribution will result in stronger antibacterial action. However, fast release is not always desirable and larger particles or a combination of smaller and larger particles will be required for lower but prolonged release of Ga^{3+} ions. Moreover, smaller nanoparticles are often found more toxic for eukaryotic cells below a certain (optimal) size [71]. On the other hand, the surface of the biomaterial is also very important, and more homogeneous Ga distribution on HAp might enable better growth of mammalian cells on the surface of the Ga@HAp material. Yarema et al. have recently found a way for creating monodisperse Ga nanoparticles and controlling the thickness of their oxide shell [33]. However, this synthesis yields a stable dispersion of Ga NPs in non-polar media, whereas a stable aqueous suspension is needed for the antibacterial and toxicity studies. Furthermore, wide size distribution is actually a better representation of the industrially prepared and commercially available nanoparticles [72] and also a better representation of the realistic system that could evolve in the human body or environment [70, 73]. Hence, it is very encouraging that despite the inhomogeneous and wide size distribution of Ga nanoparticles on hydroxyapatite, for human lung fibroblasts and L929 mouse fibroblasts, the inhibitory and also the bactericidal concentrations for the Ga@HAp are below cytotoxic concentrations, which implies that the Ga@HAp biomaterial can prevent bacterial growth and enable normal growth of mammalian cells at the same time in a certain concentration range. Furthermore, for a human-friendly antibacterial protection of hydroxyapatite, in this study Ga NPs proved even better than silver nanoparticles that are most commonly used nowadays [13].

5 Conclusion

Using a low-temperature ultrasonic emulsification method we successfully developed the Ga@HAp nanocomposite, in which gallium nanospheres are coated with a thin oxide shell and attached to the hydroxyapatite nanorods. The antibacterial assay against *P. aeruginosa* and the cytotoxicity assay against human lung fibroblast IMR-90 and mouse fibroblast L929 cells revealed that the minimal inhibitory concentration of the Ga@HAp for *P. aeruginosa* was non-toxic to mammalian cells and a useful range of concentrations, in which the Ga@HAp exhibited high antibacterial activity and low toxicity, was determined. This range was much wider than for a comparable nanocomposite of hydroxyapatite and silver nanoparticles. The ion-release study confirmed the expected release of Ga^{3+} ions from the the Ga@HAp, which contributed notably to its antibacterial action. The obtained results imply that the antibacterial properties of Ga@HAp are based on a local release of Ga^{3+} ions from the Ga nanoparticles. The high antibacterial activity and biocompatibility make the Ga@HAp nanocomposite a very promising new biomaterial for future biomedical applications (tissue engineering, wound healing, bone fracture repair, prevention of infections during implantation) and a new direction towards an advanced biomaterial that can stimulate tissue growth while being self-protected against infection at the same time.

Acknowledgments The authors appreciate the financial support of the Slovenian Research Agency (financing of young researchers) and the SCOPES (Scientific co-operation between Eastern Europe and Switzerland) project no. IZ73Z0_152327.

Compliance with ethical standards

Conflict of interest The authors declare that they have no conflict of interest.

References

1. Gray F, Kramer DA, Bliss JD. Gallium and Gallium compounds. In: Howe-Grant M, Kirk RE, editors. Kirk-Othmer encyclopedia of chemical technology. 4th edn. New York: John Wiley & Sons; 1998. pp. 158–66.
2. Greenwood NN, Earnshaw A. Aluminium, Gallium, Indium and Thallium. In: Greenwood NN, Earnshaw A, editors. Chemistry of the elements. 2nd edn. Oxford: Butterworth-Heinemann; 1997. pp. 216–67.
3. Xu Q, Qudalov N, Guo Q, Jaeger H, Brown E. Effect of oxidation on the mechanical properties of liquid gallium and eutectic gallium-indium. Phys Fluids. 2012;24(6):063101.
4. Soares BF, MacDonald KF, Fedotov VA, Zheludev NI. Light-induced switching between structural forms with different optical properties in a single gallium nanoparticulate. Nano Lett. 2005;5(10):2104–07.

5. Parravicini GB, Stella A, Ghigna P, et al. Extreme undercooling (down to 90 K) of liquid metal nanoparticles. Appl Phys Lett. 2006;89:033123.
6. Knight MW, Coenen T, Yang Y, et al. Gallium plasmonics: deep subwavelength spectroscopic imaging of single and interacting gallium nanoparticles. ACS Nano. 2015;9(2):2049–60.
7. Bernstein LR. Mechanisms of Therapeutic Activity for Gallium. Pharmacol Rev. 1998;50(4):665–82.
8. Collery P, Keppler B, Madoulet C, Desoize B. Gallium in cancer treatment. Crit Rev. Oncol Hemat. 2002;42(3):283–96.
9. Chitambar CR. Medical applications and toxicities of gallium compounds. Int J Environ Res Public Health. 2010;7(5):2337–61.
10. Kaneko Y, Thoendel M, Olakanmi O, Britigan BE, Singh PK. The transition metal gallium disrupts Pseudomonas aeruginosa iron metabolism and has antimicrobial and antibiofilm activity. J Clin Invest. 2007;117(4):877–88.
11. Brouqui P, Rousseau MC, Stein A, Drancourt M, Raoult D. Treatment of Pseudomonas aeruginosa-Infected Orthopedic Prostheses with Ceftazidime-Ciprofloxacin Antibiotic Combination. Antimicrob Agents Chemother. 1995;39(11):2423–25.
12. Sirelkhatim A, Mahmud S, Seeni A, et al. Review on zinc oxide nanoparticles: antibacterial activity and toxicity mechanism. Nano-Micro Lett. 2015;7(3):219–42.
13. Chernousova S, Epple M. Silver as antibacterial agent: ion, nanoparticle, and metal. Angew Chem Int Edit. 2013;52(6):1636–53.
14. Seil JT, Webster TJ. Antimicrobial applications of nanotechnology: methods and literature. Int J Nanomed. 2012;7:2767–81.
15. Dizaj SM, Lotfipour F, Barzegar-Jalali M, Zarrintan MH, Adibkia K. Antimicrobial activity of the metals and metal oxide nanoparticles. Mater Sci Eng C. 2014;44:278–84.
16. Huh AJ, Kwon YJ. "Nanoantibiotics": A new paradigm for treating infectious diseases using nanomaterials in the antibiotics resistant era. J Control Release. 2011;156(2):128–45.
17. Dorozhkin SV. Calcium orthophosphates: applications in nature, biology, and medicine. Singapore: Pan Stanford; 2012.
18. Dorozhkin SV. Calcium orthophosphates in dentistry. J Mater Sci-Mater M. 2013;24(6):1335–63.
19. Wang P, Zhao L, Liu J, Weir MD, Zhou X, Xu HHK. Bone tissue engineering via nanostructured calcium phosphate biomaterials and stem cells. Bone Res. 2014;2:14017.
20. Vukomanović M, Repnik U, Zavašnik-Bergant T, Kostanjšek R, Škapin Srečo D, Suvorov D. Is nano-silver safe within bioactive hydroxyapatite composites? ACS Biomater Sci Eng. 2015;1(10):935–46.
21. Vukomanović M, Logar M, Škapin SD, Suvorov D. Hydroxyapatite/gold/arginine: designing the structure to create antibacterial activity. J Mater Chem B. 2014;2(11):1557–64.
22. Repetto G, Peso A. Gallium, Indium, and Thallium. In: Bingham E, Cohrssen B, editors. Patty's toxicology. 6th edn. New York: John Wiley & Sons; 2012. pp. 257–354.
23. Yu HS, Liao WT. Gallium: Environmental Pollution and Health Effects. In: Nriagu JO, editor. Encyclopedia of environmental health. Burlington: Elsevier; 2011. pp. 829–33.
24. Wataha JC, Nakajima H, Hanks CT, Okabe T. Correlation of cytotoxicity with element release from mercury- and gallium-based dental alloys in vitro. Dent Mater. 1994;10(5):298–303.
25. Kubásek J, Vojtěch D, Lipov J, Ruml T. Structure, mechanical properties, corrosion behavior and cytotoxicity of biodegradable Mg-X (X=Sn, Ga, In) alloys. Mater Sci Eng C. 2013;33(4):2421–32.
26. Wataha JC, Hanks CT, Craig RG. The in vitro effects of metal cations on eukaryotic cell metabolism. J Biomed Mater Res. 1991;25(9):1133–49.
27. Schedle A, Samorapoompichit P, Rausch-Fan XH, et al. Response of L-929 fibroblasts, human gingival fibroblasts, and human tissue mast cells to various metal cations. J Dent Res. 1995;74(8):1513–20.
28. Schmalz G, Arenholt-Bindslev D, Pfüller S, Schweikl H. Cytotoxicity of metal cations used in dental cast alloys. ATLA-Altern Lab Anim. 1997;25(3):323–30.
29. Milheiro A, Nozaki K, Kleverlaan CJ, Muris J, Miura H, Feilzer AJ. In vitro cytotoxicity of metallic ions released from dental alloys. Odontology. 2016;104(2):136–42.
30. Qiu K, Lin W, Zhou F, et al. Ti-Ga binary alloys developed as potential dental materials. Mater Sci Eng C. 2014;34:474–83.
31. Lu Y, Hu Q, Lin Y, et al. Transformable liquid-metal nanomedicine. Nat Commun. 2015;6:10066.
32. Tsai KL, Dye JL. Synthesis, Properties, and characterization of nanometer-size metal particles by homogeneous reduction with alkalides and electrides in aprotic solvents. Chem Mater. 1993;5(13):540–46.
33. Yarema M, Wörle M, Rossell MD, et al. Monodisperse colloidal gallium nanoparticles: synthesis, low temperature crystallization, surface plasmon resonance and Li-ion storage. J Am Chem Soc. 2014;136:12422–30.
34. Li YB, Bando Y, Golberg D, Liu ZW. Ga-filled single-crystalline MgO nanotube: Wide-temperature range nanothermometer. Appl Phys Lett. 2003;83(5):999–1001.
35. Nisoli M, Stagira S, De Silvestri S, et al. Ultrafast electronic dynamics in solid and liquid gallium nanoparticles. Phys Rev Lett. 1997;78(18):3575–78.
36. Malvezzi AM, Patrini M, Stella A, Tognini P, Cheyssac P, Kofman R. Linear and nonlinear optical characterization of Ga nanoparticle monolayers. Mater Sci Eng C. 2001;15:33–5.
37. Meléndrez MF, Cárdenas G, Arbiol J. Synthesis and characterization of gallium colloidal nanoparticles. J Colloid Interf Sci. 2010;346(2):279–87.
38. Han ZH, Yang B, Qi Y, Cumings J. Synthesis of low-melting-point metallic nanoparticles with an ultrasonic nanoemulsion method. Ultrasonics. 2011;51(4):485–8.
39. Friedman H, Reich S, Popovitz-Biro R, et al. Micro- and nanospheres of low melting point metals and alloys, formed by ultrasonic cavitation. Ultrason Sonochem. 2013;20(1):432–44.
40. Kumar VB, Gedanken A, Kimmel G, Porat Z. Ultrasonic cavitation of molten gallium: formation of micro- and nano-spheres. Ultrason Sonochem. 2014;21(3):1166–73.
41. Yamaguchi A, Mashima Y, Iyoda T. Reversible size control of liquid-metal nanoparticles under ultrasonication. Angew Chem Int Edit. 2015;54:12809–813.
42. Valappil SP, Ready D, Abou Neel EA, et al. Controlled delivery of antimicrobial gallium ions from phosphate-based glasses. Acta Biomater. 2009;5(4):1198–1210.
43. Zeimaran E, Pourshahrestani S, Djordjevic I, et al. Antibacterial properties of poly (octanediol citrate)/gallium-containing bioglass composite scaffolds. J Mater Sci-Mater M. 2016;27(1):18.
44. Sahdev R, Ansari TI, Higham SM, Valappil SP. Potential use of gallium-doped phosphate-based glass material for periodontitis treatment. J Biomater Appl. 2015;30(1):85–92.
45. Pourshahrestani S, Zeimaran E, Adib Kadri N, et al. Gallium-containing mesoporous bioactive glass with potent hemostatic activity and antibacterial efficacy. J Mater Chem B. 2016;4(1):71–86.
46. Mellier C, Fayon F, Schnitzler V, et al. Characterization and properties of novel gallium-doped calcium phosphate ceramics. Inorg Chem. 2011;50(17):8252–60.
47. Mellier C, Fayon F, Boukhechba F, et al. Design and properties of novel gallium-doped injectable apatitic cements. Acta Biomater. 2015;24:322–32.
48. Jevtić M, Mitrić M, Škapin SD, Jančar B, Ignjatović N, Uskoković D. Crystal structure of hydroxyapatite nanorods synthesized by sonochemical homogeneous precipitation. Cryst Growth Des. 2008;8(7):2217–22.

49. Miranda M, Fernández A, Díaz M, et al. Silver-hydroxyapatite nanocomposites as bactericidal and fungicidal materials. Int J Mater Res. 2010;101(1):122–27.
50. Marczenko Z, Balcerzak M. Separation, Pre-concentration and Spectrophotometry in Inorganic Analysis. 1st edn. Amsterdam: Elsevier; 2001.
51. Miklavič Š, Kogovšek P, Hodnik V, et al. The Pseudomonas aeruginosa RhlR-controlled aegerolysin RahU is a low-affinity rhamnolipidbinding protein. FEMS Microbiol Lett. 2015;362: fnv069.
52. Wu PC, Kim TH, Brown AS, Losurdo M, Bruno G, Everitt HO. Real-time plasmon resonance tuning of liquid Ga nanoparticles by in situ spectroscopic ellipsometry. Appl Phys Lett. 2007;90 (10):103119.
53. Tsay SF. Relation between the β and rapidly quenched liquid phases of gallium. Phys Rev B. 1994;50(1):103–07.
54. Bohren C, Huffman DR. Absorption and Scattering of Light by Small Particles. New York: Wiley Interscience; 1998.
55. Vukomanović M, Bračko I, Poljanšek I, Uskoković D, Škapin SD, Suvorov D. The growth of silver nanoparticles and their combination with hydroxyapatite to form composites via a sonochemical approach. Cryst Growth Des. 2011;11:3802–12.
56. Takamiya AS, Monteiro DR, Bernabé DG, Gorup LF, Camargo ER, Gomes-Filho JE, Oliveira SHP. In vitro and in vivo toxicity evaluation of colloidal silver nanoparticles used in endodontic treatments. J Endodont. 2016;42(6):953–60.
57. AshaRani PV, Mun GLK, Hande MP, Valiyaveettil S. Cytotoxicity and genotoxicity of silver nanoparticles in human cells. ACS Nano. 2009;3(2):279–90.
58. Rzhepishevska O, Ekstrand-Hammarström B, Popp M, et al. The antibacterial activity of Ga^{3+} is influenced by ligand complexation as well as the bacterial carbon source. Antimicrob Agents Ch. 2011;55(12):5568–80.
59. Bonchi C, Imperi F, Minandri F, Visca P, Frangipani E. Repurposing of gallium-based drugs for antibacterial therapy. BioFactors. 2014;40:303–12.
60. Durán N, Durán M, de Jesus MB, Seabra AB, Fávaro WJ, Nakazato G. Silver nanoparticles: a new view on mechanistic aspects on antimicrobial activity. Nanomed-Nanotechnol. 2016;12:789–99.
61. Kora AJ, Arunachalam J. Assessment of antibacterial activity of silver nanoparticles on Pseudomonas Aeruginosa and its mechanism of action. World J Microb Biot. 2011;27(5):1209–16.
62. Tzitrinovich Z, Lipovsky A, Gedanken A, Lubart R. Visible light-induced OH radicals in Ga_2O_3: an EPR study. Phys Chem Chem Phys. 2013;15(31):12977–81.
63. Valko M, Morris H, Cronin MTD. Metals, toxicity and oxidative stress. Curr Med Chem.. 2005;12(10):1161–208.
64. Lemire JA, Harrison JJ, Turner RJ. Antimicrobial activity of metals: mechanisms, molecular targets and applications. Nat Rev Microbiol. 2013;11(6):371–84.
65. He W, Zhou YT, Wamer WG, Boudreau MD, Yin JJ. Mechanisms of the pH dependent generation of hydroxyl radicals and oxygen induced by Ag nanoparticles. Biomaterials. 2012;33 (30):7547–55.
66. Bériault R, Hamel R, Chenier D, Mailloux RJ, Joly H, Appanna VD. The overexpression of NADPH-producing enzymes counters the oxidative stress evoked by gallium, an iron mimetic. BioMetals. 2007;20(2):165–76.
67. Yang M, Chitambar CR. Role of oxidative stress in the induction of metallothionein-2A and heme oxygenase-1 gene expression by the antineoplastic agent gallium nitrate in human lymphoma cells. Free Radical Bio Med. 2008;45(6):763–72.
68. Sahoo P, Murthy PS, Dhara S, Venugopalan VP, Das A, Tyagi AK. Probing the cellular damage in bacteria induced by GaN nanoparticles using confocal laser Raman spectroscopy. J Nanopart Res. 2013;15:1841.
69. Kaptay G. On the size and shape dependence of the solubility of nano-particles in solutions. Int J Pharm. 2012;430:253–7.
70. Reidy B, Haase A, Luch A, Dawson KA, Lynch I. Mechanisms of silver nanoparticle release, transformation and toxicity: a critical review of current knowledge and recommendations for future studies and applications. Materials. 2013;6:2295–350.
71. Shang L, Nienhaus K, Nienhaus GU. Engineered nanoparticles interacting with cells: size matters. J Nanobiotechnology. 2014;12 (5):1–11.
72. Berhanu D, Valsami-Jones E. Nanotoxicity: are we confident for modelling? - an experimentalist's point of view. In: Leszczynski J, Puzyn T, editors. Towards efficient designing of safe nanomaterials: innovative merge of computational approaches and experimental techniques. Royal Society of Chemistry; 2012. pp. 54–68.
73. Glover RD, Miller JM, Hutchison JE. Generation of metal nanoparticles from silver and copper objects: nanoparticle dynamics on surfaces and potential sources of nanoparticles in the environment. ACS Nano. 2011;5(11):8950–7.